J Seismol (2017) 21:1277–1284
DOI 10.1007/s10950-017-9660-6

SHORT COMMUNICATION

Factors controlling high-frequency radiation from extended ruptures

Igor A. Beresnev

Received: 27 December 2016 / Accepted: 27 March 2017 / Published online: 5 April 2017

Abstract Small-scale slip heterogeneity or variations in rupture velocity on the fault plane are often invoked to explain the high-frequency radiation from earthquakes. This view has no theoretical basis, which follows, for example, from the representation integral of elasticity, an exact solution for the radiated wave field. The Fourier transform, applied to the integral, shows that the seismic spectrum is fully controlled by that of the source time function, while the distribution of final slip and rupture acceleration/deceleration only contribute to directivity. This inference is corroborated by the precise numerical computation of the full radiated field from the representation integral. We compare calculated radiation from four finite-fault models: (1) uniform slip function with low slip velocity, (2) slip function spatially modulated by a sinusoidal function, (3) slip function spatially modulated by a sinusoidal function with random roughness added, and (4) uniform slip function with high slip velocity. The addition of "asperities," both regular and irregular, does not cause any systematic increase in the spectral level of high-frequency radiation, except for the creation of maxima due to constructive interference. On the other hand, an increase in the maximum rate of slip on the fault leads to highly amplified high frequencies, in accordance with the prediction on the basis of a simple point-source treatment of the fault. Hence, computations show that the temporal rate of slip, not the spatial heterogeneity on faults, is the predominant factor forming the high-frequency radiation and thus controlling the velocity and acceleration of the resulting ground motions.

Keywords Earthquake radiation · Ground motions · Representation theorem · Source time function · Heterogeneous slip

I. A. Beresnev (✉)
Department of Geological and Atmospheric Sciences, Iowa State University, 253 Science I, 2237 Osborn Drive, Ames, IA 50011-3212, USA
e-mail: beresnev@iastate.edu

1 Problem formulation

A view often expressed in modeling seismic radiation from finite faults is that high frequencies are generated by small-scale variations or roughness in static slip, slip velocity, or rupture velocity (acceleration and deceleration) over the fault plane (Madariaga 1977, 1983; Somerville et al. 1999, p. 60; Shi and Day 2013). A consequence, for example, often assumed in the inversion of strong-motion records for slip distribution on ruptures of major earthquakes is that, once data have been low-pass filtered, the static-slip heterogeneity can be neglected (Beresnev 2003, p. 2451). The latter assumption probably originates from the classic work of Haskell (1964, equation 62 and p. 1830), who inferred increased high-frequency-energy content in radiated spectra when statistically independent "patches" of coherent radiation were introduced on the fault plane.

Understanding the source of high frequencies in earthquake motion is important from the practical standpoint, as they control the velocity and acceleration of ground shaking used in characterizing seismic hazard. To pinpoint the origin of high frequencies from the theoretical standpoint, it is useful to turn to the representation theorem of elasticity. The theorem prescribes the exact wave field radiated by a displacement discontinuity in an elastic space (Aki and Richards 1980, equation 14.37):

$$u_i(\mathbf{x},t)=\frac{\mu}{4\pi\rho}\iint\left[\begin{array}{l}\dfrac{30\gamma_i n_p\gamma_p\gamma_q v_q-6v_i n_p\gamma_p-6n_i\gamma_q v_q}{R^4}\int_{R/\alpha}^{R/\beta}t'\,\Delta u\left(\xi,t-t'\right)dt'\\ +\dfrac{12\gamma_i n_p\gamma_p\gamma_q v_q-2v_i n_p\gamma_p-2n_i\gamma_q v_q}{\alpha^2R^2}\Delta u\left(\xi,t-\dfrac{R}{\alpha}\right)\\ -\dfrac{12\gamma_i n_p\gamma_p\gamma_q v_q-3v_i n_p\gamma_p-3n_i\gamma_q v_q}{\beta^2R^2}\Delta u\left(\xi,t-\dfrac{R}{\beta}\right)+\dfrac{2\gamma_i n_p\gamma_p\gamma_q v_q}{\alpha^3R}\Delta u\left(\xi,t-\dfrac{R}{\alpha}\right)\\ -\dfrac{2\gamma_i n_p\gamma_p\gamma_q v_q-v_i n_p\gamma_p-n_i\gamma_q v_q}{\beta^3R}\Delta u\left(\xi,t-\dfrac{R}{\beta}\right)\end{array}\right]d\sum(\xi).\qquad(1)$$

Here, $u_i(\mathbf{x},t)$ is the ith component of the radiated displacement; $\mathbf{x}$ and $\boldsymbol{\xi}$ are the coordinates of the observation point and the point on the fault surface, respectively, $\Delta\mathbf{u}(\boldsymbol{\xi},t)=\mathbf{u}(\boldsymbol{\xi},t)|_{\Sigma^+}-\mathbf{u}(\boldsymbol{\xi},t)|_{\Sigma^-}$ is the vector of displacement discontinuity across the fault plane with sides Σ^+ and Σ^-, $\Delta\mathbf{u}(\boldsymbol{\xi},t)=\mathbf{n}\Delta u(\boldsymbol{\xi},t)$, $\Delta u(\boldsymbol{\xi},t)$ is the slip ("source time") function, $\Delta u(\boldsymbol{\xi},t)$ is its time derivative (the slip rate), $\mathbf{n}$ is the unit vector in the direction of slip, $\boldsymbol{\nu}$ is the unit normal to the fault pointing from Σ^- to Σ^+, $R=|\mathbf{x}-\boldsymbol{\xi}|$, $\boldsymbol{\gamma}=(\mathbf{x}-\boldsymbol{\xi})/R$, α and β are the P- and S-wave propagation speeds, and μ and ρ are the shear modulus and density of the medium. The double integration in Eq. (1) is carried over the fault plane $\Sigma(\boldsymbol{\xi})$; the summation convention is assumed for repeated subscripts. We have also used the explicit compact convolution integral in the first term in the integrand instead of the long notation through the function $F(t)$ as in the original equation (14.37) of Aki and Richards (Beresnev 2017).

To acquire the Fourier spectrum of equation (1), we first write $\int_{R/\alpha}^{R/\beta}t'\Delta u\left(\xi,t-t'\right)\,dt'=\int_{-\infty}^{\infty}t_1\left(t'\right)\Delta u\left(\xi,t-t'\right)dt'$, where

$$t_1\left(t'\right)=\begin{cases}t', & \dfrac{R}{\alpha}\le t'\le\dfrac{R}{\beta}\\ 0 \text{ elsewhere.}\end{cases}\qquad(2)$$

Then, for a source time function in the form of a radially propagating rupture,

$$\Delta u(\boldsymbol{\xi},t)=U(\boldsymbol{\xi})\Delta u\left(t-\frac{r}{v}\right),\qquad(3)$$

where $U(\boldsymbol{\xi})$ is the distribution of the final-slip values over the fault plane, $r=|\boldsymbol{\xi}-\boldsymbol{\xi}_0|$, $\boldsymbol{\xi}_0$ is the hypocenter point, and v is the rupture-propagation speed, applying the time-shift, derivative, and convolution theorems, we obtain the Fourier transform of Eq. (1):

$$u_i(\mathbf{x},\omega)=\frac{\mu}{4\pi\rho}\Delta u(\omega)\iint U(\xi)e^{-i\omega\frac{r}{v}}\left[\begin{array}{l}\dfrac{30\gamma_i n_p\gamma_p\gamma_q v_q-6v_i n_p\gamma_p-6n_i\gamma_q v_q}{R^4}t_1(\omega)\\ +\dfrac{12\gamma_i n_p\gamma_p\gamma_q v_q-2v_i n_p\gamma_p-2n_i\gamma_q v_q}{\alpha^2R^2}e^{-i\omega\frac{R}{\alpha}}\\ -\dfrac{12\gamma_i n_p\gamma_p\gamma_q v_q-3v_i n_p\gamma_p-3n_i\gamma_q v_q}{\beta^2R^2}e^{-i\omega\frac{R}{\beta}}+\dfrac{2\gamma_i n_p\gamma_p\gamma_q v_q}{\alpha^3R}i\omega e^{-i\omega\frac{R}{\alpha}}\\ -\dfrac{2\gamma_i n_p\gamma_p\gamma_q v_q-v_i n_p\gamma_p-n_i\gamma_q v_q}{\beta^3R}i\omega e^{-i\omega\frac{R}{\beta}}\end{array}\right]d\sum(\xi).\qquad(4)$$

Here, $\Delta u(\omega)$ and $t_1(\omega)$ are the Fourier transforms of $\Delta u(t)$ and $t_1(t)$, respectively, and we have assumed that the temporal function $\Delta u(t)$ does not depend on the position on the fault plane. The function $t_1(\omega)$ evaluates analytically:

$$t_1(\omega) = \frac{1}{\omega}\left[e^{-i\omega\frac{R}{\beta}}\left(i\frac{R}{\beta}+\frac{1}{\omega}\right)-e^{-i\omega\frac{R}{\alpha}}\left(i\frac{R}{\alpha}+\frac{1}{\omega}\right)\right], \quad (5)$$

from which also $t_1(\omega=0) = \frac{R^2}{2}\left(\frac{1}{\beta^2}-\frac{1}{\alpha^2}\right)$.

Equation (4) shows that the spectrum of the radiated displacement is that of the source time function $\Delta u(\omega)$ modified by a factor representing an integral over the fault plane, with the integrand equal to $U(\xi)$ multiplied by a factor of complicated form in the brackets. The integral describes the frequency-dependent directivity, caused by the interference of the waves radiated to an observation point from different parts of the fault. There is no mechanism by which this integral would preferentially amplify high frequencies. This inference rules out heterogeneity in static slip $U(\xi)$ as the systematic source of high frequencies.

The enrichment of the spectra in high-frequency energy through the introduction of asperities, described by Haskell (1964), may be an artifact caused by the author's treatment of the patches of coherent radiation as independent small sources and the assumption of additivity of their power spectra. Radiation from smaller sources has higher corner frequencies, which should result in increased high-frequency content after summation.

One finds direct evidence of the increase in high-frequency radiation simply by subdivision of the continuous fault plane into a set of smaller "subfaults" in the study by Boore and Joyner (1978). Both Haskell and Boore and Joyner employ simple analytical solutions for the emitted wave field allowed by their neglect of all near-field terms. Far-field emission from smaller sources has higher corner frequencies, which results in increased high-frequency content of the total radiation from all subfaults relative to the "smooth" continuous rupture. Although Boore and Joyner randomize both static slips and the lengths of their fault segments, the latter are still characterized by a smaller mean length relative to that of the fault as a whole (Boore and Joyner 1978, p. 287). The smaller the length, the greater the corner frequency of subfault radiation (Boore and Joyner 1978, Fig. 9), with the ensuing enhancement in high-frequency energy (Boore and Joyner 1978, Fig. 7). Such enhancement is not the effect of incoherence of radiation from adjacent subfaults (Haskell) or randomness in the distribution of slip over the fault plane (Boore and Joyner) but rather a consequence of the simplified methodology used based on the analytical representation of fault radiation through a system of independent small sources with only the far-field terms retained. Conversely, Eq. (1) presents the general case that uses continuous integration of all terms for the radiated field.

Equation (4) demonstrates that the main contributor of high frequencies to the fault radiation is the source time function itself, while the distribution in static slip $U(\xi)$ merely plays a modulating role. However, the degree of the influence of $U(\xi)$ can only be ascertained by precise numerical integration, to which we proceed.

2 Numerical calculation of radiated wave field

We follow the procedure of the numerical computation of the displacement field $u_i(\mathbf{x}, t)$ in Eq. (1) described by Beresnev (2017), which can be outlined as follows. The analytical form of slip $\Delta u(\xi, t)$ is taken as

$$\Delta u(\xi,t) = \begin{cases} 0, & t<0 \\ U(\xi)\left[1-\left(1+\frac{t}{\tau}\right)e^{-t/\tau}\right], & t\geq 0 \end{cases} \quad (6)$$

where the parameter τ determines how fast the fault dislocation rises to its final value (Beresnev and Atkinson 1997, equation 6). However, merely serving as a characteristic time scale in Eq. (6), the quantity τ cannot be considered as a controlling physical parameter unless it is substituted by a quantity having clear physical meaning and related to the process of faulting. This is achieved through the parameter v_{max} introduced in the following.

The temporal form of slip represented by Eq. (6) is a reasonable choice, because a point source with the same time function radiates exactly the commonly observed "ω^{-2}" Fourier spectrum in the far field, with the frequency corner ω_c defined by τ,

$$|u_{iPS}(\mathbf{x},\omega)| = CM_0\frac{1}{1+\left(\frac{\omega}{\omega_c}\right)^2}, \quad (7)$$

$$\omega_c \equiv \frac{1}{\tau}, \tag{8}$$

(Beresnev and Atkinson 1997, equations 6 and 11). Here, $M_0 = \mu U_0 A$ is the seismic moment, μ is the shear modulus of the medium, U_0 is the average total slip at the source, A is the rupture area, and C is a frequency-independent factor. The temporal function (6) is sometimes referred to as the "Ohnaka ramp" (Anderson and Richards 1975, p. 353), after Ohnaka (1973, equation 16) who introduced it on entirely different grounds. If v_{max} is the maximum velocity of the dislocation rise, then τ is

$$\tau = \frac{U_0}{e v_{max}}, \tag{9}$$

where e is the base of the natural logarithm (Beresnev 2001, p. 398). The physical quantity v_{max} then substitutes the yet formally defined time scale τ as a governing physical parameter of the faulting. $U(\xi)$ and v_{max} become the two free, physically grounded parameters of the model. With $\Delta u(\xi, t)$ as in Eq. (6), the convolution integral in the first term of Eq. (1) evaluates analytically, and the integrand is completely defined. The double integration in Eq. (1) is carried out to the precision of eight decimal digits. The hypocenter is placed at the center of a vertical right-lateral strike-slip fault, for which the geometric coefficients $\gamma_i n_p \gamma_p \gamma_q \nu_q$, $\nu_i n_p \gamma_p$, and $n_i \gamma_q \nu_q$ in the integrand reduce to simple analytical forms. The elastic constants are taken as $\alpha = 5$ km/s, $\beta = \alpha/\sqrt{3}$, $\rho = 2700$ kg/m^3, and the rupture-propagation speed as $v = 0.8\beta$. Fault dimensions are 3.4 km × 3.4 km, which, according to the empirical relation $\log A = -3.49 + 0.91\, M_w$, where M_w is the moment magnitude (Wells and Coppersmith 1994, Table 2A), corresponds to a M_w 5 earthquake. The average fault offset $U_0 = 0.14$ m then follows from combining the definitions of the seismic moment and that of the moment magnitude, $M_w = (2/3) \log M_0 - 10.7$. The computed displacement time histories are low-pass filtered with the cut-off frequency of 45 Hz and then numerically differentiated twice to obtain the acceleration waveforms.

It follows from Eqs. (7)–(9) and the definition of the moment that the high-frequency ($\omega > \omega_c$) spectrum is controlled by v_{max}:

$$|u_{iPS}(\mathbf{x}, \omega)|_{hf} = CA\mu e^2 \frac{v_{max}^2}{\omega^2 U_0}. \tag{10}$$

Consequently, v_{max}, as the physically meaningful parameter of the source time function, but not the fault heterogeneity, can be expected to be the most significant factor responsible for the formation of high-frequency radiation from faults. Equation (10) has been obtained by treating the fault as a point source, with only the far-field terms considered; however, the suggested behavior can now be verified through the direct computations of the full integral (1).

3 Effects of maximum slip velocity and slip irregularities on radiated spectra

Figure 1 shows the geometry of the problem, depicting the fault plane, the location of the origin O of the cartesian coordinate system, and the orientation of the axes. All computations have been performed for an observation point A having the coordinates {0, 200, 200} m. To examine the effects of the maximum slip rate, on one hand, and fault-slip heterogeneities, on the other, complete fault-perpendicular components $u_2(\mathbf{x}, t)$ of the displacement field were calculated for four models, all having the same average total slip and thus the same seismic moment. The x_2-component was chosen because it was found to be the largest. Model 1 (the "base" model: low slip velocity, homogeneous slip) has $v_{max} = 1$ m/s and a constant total offset in Eq. (6) over the entire fault plane, $U(\xi) = U_0$. Model 2 (low average slip velocity, slip disturbed in a regular manner) keeps the same $v_{max} = 1$ m/s but superimposes a sinusoidal modulation on the constant U_0 from model 1 with the wavelength equal to one quarter of the side L of the fault and the amplitude of $0.5U_0$. Thus, the final offset in Eq. (6) for model 2 is $U(\xi) = U_0(1 + 0.5 \sin k\xi_1 \sin k\xi_3)$, where $k = 2\pi/\lambda$ and $\lambda = L/4$. The parameter τ is still determined by Eq. (9) with the mean displacement U_0 and remains fixed: the source time function (6) is thus scaled by $U(\xi)$ keeping the same $v_{max} = 1$ m/s on

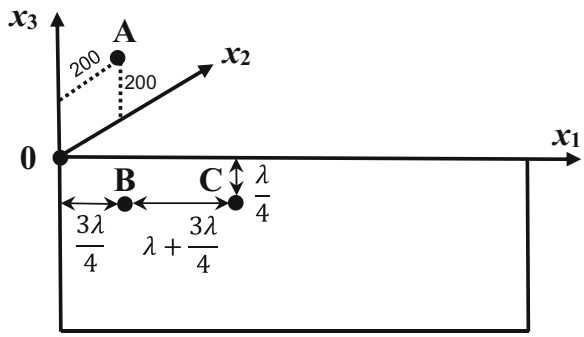

Fig. 1 Geometry of the problem (not to scale)

average. Model 3 (low average slip velocity, slip disturbed in both regular and stochastic manner) still retains v_{max} = 1 m/s in the same procedure but superimposes a random component on the slip from model 2: $U(\boldsymbol{\xi}) = U_0[1 + 0.5 \sin k\xi_1 \sin k\xi_3 + 0.5\eta(\xi_1, \xi_3)]$, where the random variable $\eta(\xi_1, \xi_3)$ is drawn from a normal distribution with zero mean and standard deviation of 0.06, constrained to equal −1 if its value accidentally fell below −1. In models 2 and 3, therefore, both the final slip and v_{max} are heterogenized. The quantity $U(\boldsymbol{\xi})$ in model 3 was realistically generated on a grid with a step of $\lambda/20$ in each direction ξ_1 and ξ_3 on the fault plane and then interpolated during the numerical evaluation of integral (1). With $\lambda/20 \approx 43$ m, the largest wavenumber in the resulting randomized slip is on the order of $k_{max} \approx 2\pi/43 \approx 0.15$ m^{-1}; the maximum frequency that this slip can generate can then be estimated as $f_{max} \approx k_{max}v/2\pi \approx 55$ Hz. Figure 2 plots the grid of $U(\boldsymbol{\xi})$ over the fault resulting from model 3. Finally, model 4 is the "base" model 1 in which the maximum slip rate is increased by a factor of two, v_{max} = 2 m/s (high slip velocity, homogeneous slip).

3.1 Effects of slip irregularities

Figure 3 displays the ratio of the modulus of the Fourier spectrum of the particle-acceleration time history at the observation point computed for model 2 to that for model 1. We found that the evaluation of Fourier spectra of acceleration was more stable than that of displacement, even after cosine tapering, because of the Gibbs

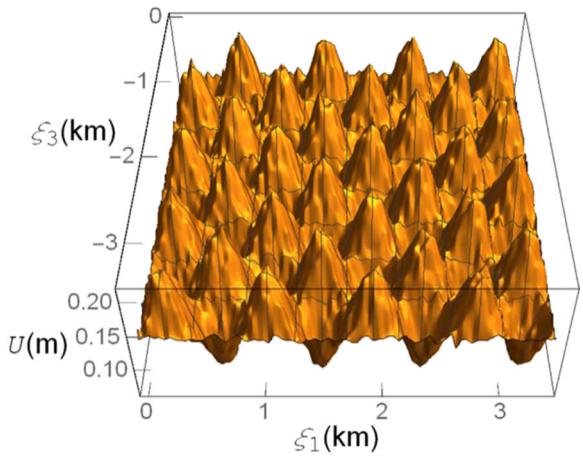

Fig. 2 Distribution of both sinusoidally and stochastically disturbed total slip resulting from model 3

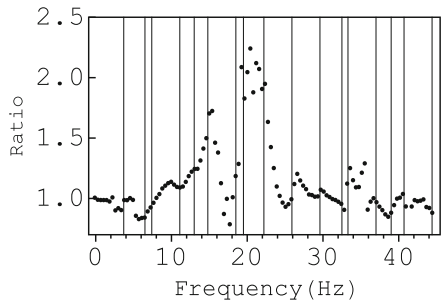

Fig. 3 Ratio of the moduli of Fourier spectra of radiation of model 2 to model 1. The *vertical lines* indicate the frequencies of constructive interference, calculated in the text, of the waves from the asperities centered at B and C in Fig. 1

phenomenon affecting the spectra of displacement due to a significant constant offset at the end of the traces. Owing to the time differentiation that removes the offset, these effects were absent from the acceleration traces. It is seen from Fig. 3 that the introduction of the sinusoidal modulation (slip "asperities") in model 2 did not lead to any systematic enhancement in high-frequency content (increase in the ratio from one), except for the appearance of isolated peaks. The following simple calculation helps explain the origin of the peaks.

Asperities emit waves when the motion on the rest of the fault has already ceased. Constructive interference at the observation point will cause additional amplification relative to the case of uniform slip. Consider, for example, the two leftmost asperities in the upper row of the fault (Fig. 2; disregard the superimposed noise). Their centers are marked B and C in Fig. 1, having the coordinates $\{3\lambda/4, 0, -\lambda/4\}$ and $\{\lambda + 3\lambda/4, 0, -\lambda/4\}$, respectively, where $\lambda = L/4 = 850$ m. From the coordinates, the distances are 785.2 m between points B and A and 1556.5 m between points C and A, giving the difference ΔR = 771.3 m in the paths of wave travel from the asperities B and C to the observation point. The waves will interfere constructively if ΔR is a multiple of *P*- and *S*-wavelengths: $\Delta R = n\lambda_P$ and $\Delta R = n\lambda_S$, from which the frequencies of constructive interference are deduced as $f = n\alpha/\Delta R$ and $f = n\beta/\Delta R$. All the frequencies obtained from these two relationships are plotted as vertical lines in Fig. 3. They coincide with some peaks (only two asperities have been considered), indicating that the maxima are most likely caused by constructive interference. The strongest peak may be associated with the contribution from several asperities, which is not accounted for by this simple example. The relationships also indicate that the frequencies of constructive

interference are not necessarily limited to the very large values only. This emphasizes the fact that roughness on the fault modifies radiated spectra in the wide frequency band and cannot exclusively contribute to the generation of high-frequency radiation.

Figure 4 shows the moduli of acceleration spectra of model 3 and model 1 (a) and their ratio (b). The meaning of the vertical lines is the same as in Fig. 3. The acceleration time histories, from which the spectra were calculated, are exhibited in Fig. 5 (for ease of comparison, the black line has been shifted by 0.1 g in the vertical direction). The addition of stochastic noise to the slip in model 2 did not make any appreciable difference in the radiation: the spectral ratios in Figs. 3 and 4 are nearly identical. This inference coincides with the conclusion made by Beresnev and Atkinson (1998) through the stochastic finite-fault simulation of radiation from the 1994 Northridge, California earthquake. In their study, randomizing slip distribution versus a published inverted model did not lead to a statistically greater error in the simulation of acceleration time histories near the causative fault relative to observations. As also could be expected, the added stochastic component did not create any significant additional interference patterns in Fig. 4 either. The comparison of traces in Fig. 5 shows that the addition of asperities on the fault, both regular and irregular, led to only minor effects on the acceleration time histories.

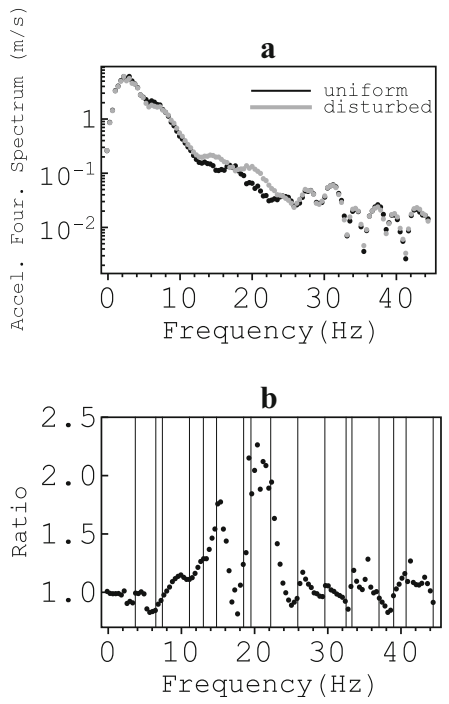

Fig. 4 **a** Moduli of Fourier spectra of radiation from model 1 (*black line*) and model 3 (*gray line*). **b** Ratio of the moduli of Fourier spectra of model 3 to model 1. The meaning of the *vertical lines* is the same as in Fig. 3

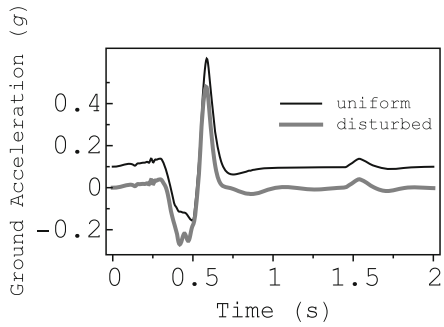

Fig. 5 Particle-acceleration time histories of radiation from model 1 (*black line*) and model 3 (*gray line*)

3.2 Effect of maximum slip velocity

Model 4 increases the maximum slip rate v_{max} on the uniform fault to 2 m/s from 1 m/s in model 1. Based on the point-source approximation, the effect of this increase on the radiated spectra can be estimated as follows. From Eqs. (8) and (9), $f_c = \omega_c/2\pi = ev_{max}/(2\pi U_0)$. Given U_0 = 0.14 m and v_{max} = 2 m/s, the corner frequency is f_c = 6.2 Hz. From Eq. (10), therefore, an increase in v_{max} by a factor of two should cause, all other parameters being equal, an amplification of the modulus of Fourier spectrum by a factor approaching four at frequencies above 6.2 Hz. Since the temporal form of displacement from a point source in the far field is simply the time derivative of $\Delta u(t)$, the same enhancement can be expected to apply to the spectrum emitted by the finite fault if $\Delta u(\omega)$ in Eq. (4) is the dominant factor. Figure 6 verifies this point by plotting

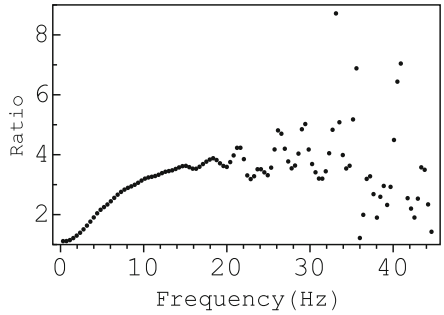

Fig. 6 Ratio of the moduli of Fourier spectra of radiation of model 4 to model 1

the ratio of the spectra of the full radiation of model 4 to model 1. The ratio gradually approaches the level of four, on average, as predicted by the point-source treatment. Note that, while neither regular nor irregular modulation of slip distribution and of maximum slip velocity led to any systematic increase in the high-frequency content, an increase in the maximum slip rate, a physical parameter of the source time function, caused a significant systematic enhancement. This corroborates the point made in the discussion of Eq. (4) that the source time function is the main source parameter controlling the strength of high-frequency radiation from ruptures.

To further demonstrate the dominant effect of $\Delta u(\omega)$ relative to the integral over the fault plane in Eq. (4), Fig. 7 plots the ratio of $\Delta u(\omega)$, calculated for the temporal function in Eq. (6), for v_{max} = 2 m/s to that for v_{max} = 1 m/s. The spectral ratio was obtained from the displacement time histories calculated from Eq. (6) through exactly the same numerical procedure as the ratios in Figs. 3, 4, and 6. Comparison with Fig. 6 shows that, indeed, the rise of the ratio to the value of four at high frequencies is entirely caused by the respective enrichment in high-frequency content in the slip function, as v_{max} doubles, while the integral in Eq. (4) is merely responsible for the modulation seen in Fig. 6 and caused by the interference effects.

4 Discussion

The effects of fault roughness, on one hand, and average peak slip velocity as the physical parameter of the temporal dependence of fault displacement, on the other, on the high-frequency spectra of fault radiation have been investigated through the numerical evaluation of the representation integral of elasticity. The latter describes the exact wave field emitted by a finite rupture. The introduction of regular and irregular spatial modulation of the source time function does not lead to any systematic enhancement in the high-frequency content relative to a uniform fault, except for the creation of spectral maxima by constructive interference of waves emanating from asperities. Conversely, the increase in peak velocity of the slip causes significant amplification of the high-frequency radiation. Based on the control of radiated spectra by that of the slip function $\Delta u(\omega)$, the level of increase and the frequency above which it occurs can be quantitatively described through a simple point-source model of the fault. The calculations show, therefore, that the average maximum rate of slip on the rupture plane, not the spatial heterogeneity of the final slip or heterogeneity of the maximum slip rate, is the principal parameter governing the level of the high-frequency part of the radiated spectra and thus the amplitudes of ground velocity and acceleration in the resulting strong seismic motions.

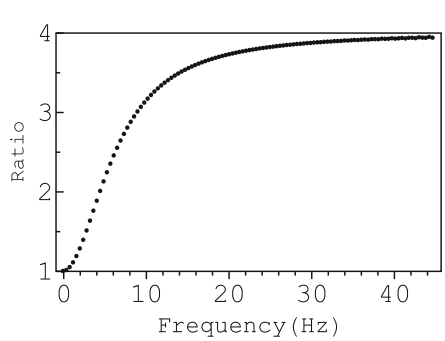

Fig. 7 Ratio of the moduli of Fourier spectra of the source time function $\Delta u(t)$ from Eq. (6) with v_{max} = 2 m/s to that with v_{max} = 1 m/s

Kame and Uchida (2008) found the source of high frequencies in an increase in slip rate following the coalescence of two cracks and the resulting stress concentration. Although their model is entirely different, the finding echoes ours: the slip rate is the primary mechanism for the generation of high frequencies.

The same conclusion about the lack of sustaining effect on high-frequency radiation will apply to the variable rupture speed. Acceleration/deceleration of rupture can be incorporated by replacing the time delay r/v in Eq. (3) by a fault-position dependent $\Delta t(r)$ of arbitrary form. The $e^{-i\omega\frac{r}{v}}$ multiplier before the brackets in the integrand of Eq. (4) will then become $e^{-i\omega\Delta t(r)}$. It is seen that variations in $\Delta t(r)$ (the timing of the arrival of rupture), as those in $U(\boldsymbol{\xi})$, will modify the directivity of radiation, described by the integral, but will not cause any systematic effects on the preferential generation of high frequencies.

Dunham et al. (2011) computed seismic radiation from a non-planar strike-slip fault with a surface topography (not to be confused with our planar strike-slip fault with heterogeneous distribution of final slip). The authors concluded that the topography roughness was a source of high-frequency radiation (Dunham et al. 2011, Fig. 7a). We do not find these results contradicting ours. Note that the authors themselves attribute the high-

frequency generation to the roughness-caused rupture acceleration/deceleration. Although they do not display the time histories of slip on their non-planar fault, they infer large stress perturbations induced by the roughness (Dunham et al. 2011, p. 2311). Recall that, in Kame and Uchida's work, such stress concentrations led to elevated slip rates. We suspect, therefore, that the increased high-frequency content, attributed by Dunham et al. to acceleration/deceleration, is rather the effect of the increased local slip rates due to stress concentrations.

Madariaga (1977) postulated that the only sources of high-frequency radiation are the "starting" and "stopping" phases. All conclusions therefore are drawn from the analysis of the first motions of these phases (Madariaga 1977, equations 34, 38, 43, 46, 50; p. 647). In Madariaga's study, these motions are discontinuous, which leads to an artificial enrichment in high frequencies. The author states that "there is no high frequency radiation while rupture proceeds at constant rupture velocity" (p. 646). This is incorrect: the statement contradicts the general relationship (4), which shows that $\Delta u(\omega)$ controls the high-frequency radiation according to Eq. (10) even if v = const. Theoretically, such radiation may be as strong as desired according to the value of v_{max}.

5 Data and resources

No data were used in this paper. All inferences were made through the numerical evaluation of the representation integral (1) as described.

Acknowledgments The paper benefited from comments and suggestions of four anonymous reviewers.

References

Aki K, Richards PG (1980) *Quantitative Seismology*, W. H. Freeman and Company

Anderson JG, Richards PG (1975) Comparison of strong ground motion from several dislocation models. Geophys J R Astron Soc 42:347–373

Beresnev IA (2001) What we can and cannot learn about earthquake sources from the spectra of seismic waves. Bull Seism Soc Am 91:397–400

Beresnev IA (2003) Uncertainties in finite-fault slip inversions: to what extent to believe? (a critical review). Bull Seism Soc Am 93:2445–2458

Beresnev IA (2017) Simulation of near-fault high-frequency ground motions from the representation theorem (in review)

Beresnev IA, Atkinson GM (1997) Modeling finite-fault radiation from the ω^n spectrum. Bull. Seism. Soc. Am. 93, 67–84

Beresnev IA, Atkinson GM (1998) Stochastic finite-fault modeling of ground motions from the 1994 Northridge, California, earthquake. I. Validation on rock sites. Bull Seism Soc Am 88:1392–1401

Boore DM, Joyner WB (1978) The influence of rupture incoherence on seismic directivity. Bull Seism Soc Am 68:283–300

Dunham EM, Belanger D, Cong L, Kozdon JE (2011) Earthquake ruptures with strongly rate-weakening friction and off-fault plasticity, part 2: Nonplanar faults. Bull Seism Soc Am 101: 2308–2322

Haskell NA (1964) Total energy and energy spectral density of elastic wave radiation from propagating faults. Bull Seism Soc Am 54:1811–1841

Kame N, Uchida K (2008) Seismic radiation from dynamic coalescence, and the reconstruction of dynamic source parameters on a planar fault. Geophys J Int 174:696–706

Madariaga R (1977) High-frequency radiation from crack (stress drop) models of earthquake faulting. Geophys J R Astron Soc 51:625–651

Madariaga R (1983) High frequency radiation from dynamic earthquake fault models. Ann Geophys 1:17–23

Ohnaka M (1973) A physical understanding of the earthquake source mechanism. J Phys Earth 21:39–59

Shi Z, Day SM (2013) Rupture dynamics and ground motion from 3-D rough-fault simulations. J Geophys Res 118:1122–1141

Somerville P, Irikura K, Graves R, Sawada S, Wald D, Abrahamson N, Iwasaki Y, Kagawa T, Smith N, Kowada A (1999) Characterizing crustal earthquake slip models for the prediction of strong ground motion. Seism Res Lett 70:59–80

Wells DL, Coppersmith KJ (1994) New empirical relationships among magnitude, rupture length, rupture width, rupture area, and surface displacement. Bull Seism Soc Am 84: 974–1002